MATERIALS CHEMISTRY
FRONTIERS

RESEARCH ARTICLE

View Article Online
View Journal | View Issue

Cite this: *Mater. Chem. Front.*, 2018, **2**, 1893

Luminescent supramolecular polymer nanoparticles for ratiometric hypoxia sensing, imaging and therapy†

Yuan-Yuan Huang,[a] Ye Tian,[a] Xiao-Qin Liu,[a] Zhongwei Niu,[a] Qing-Zheng Yang,[a] Vaidhyanathan Ramamurthy,[b] Chen-Ho Tung,[a] Yu-Zhe Chen *[a] and Li-Zhu Wu *[a]

Received 27th June 2018,
Accepted 7th August 2018

DOI: 10.1039/c8qm00309b

rsc.li/frontiers-materials

Hydrogen-bonded supramolecular polymer nanoparticles (SPNPs), serving as a ratiometric oxygen nanoprobe for hypoxia sensing and photodynamic therapy (PDT) treatment, were designed. Herein, oxygen-sensitive phosphorescent Pt(II) porphyrin moiety and oxygen-insensitive fluorescent 9,10-diphenylanthracene moiety were assembled through quadruple hydrogen bonding into SPNPs. The efficient energy transfer between the monomeric donor–acceptor pairs in the SPNPs leads to enhanced phosphorescence with long lifetimes. The resulting bright phosphorescence can realize hypoxia sensing in living cells and generate singlet oxygen efficiently in SPNPs to kill cancer cells. This is the first example of a multi-functional supramolecular polymer-based nanoprobe for ratiometric hypoxia sensing, imaging and PDT treatment.

Introduction

Molecular oxygen (O_2) is a critical component to provide metabolic energy to cells in aerobic respiration.[1] Hypoxia, a condition in which O_2 levels are below normal, is related to many diseases including cancer, neurological disorders and retinal diseases.[2] Thus, the determination of O_2 levels is of significance in diagnosing cancers and understanding the cellular function and etiology of diseases at their early stage. Optical O_2 sensors provide a powerful tool for sensing and mapping the presence of O_2 in cells and tissues.[3] Ratiometric O_2 sensing, in which the O_2 level is calculated using the ratio of O_2-insensitive fluorescence to O_2-sensitive phosphorescence, further allows more accurate measurement and avoids background interference.[3] Currently, there is great interest in the development of ratiometric optical oxygen nanoprobes by incorporating metal porphyrin complexes with conjugated polymer nanoparticles (CPNs), silica gels and quantum dots.[4–7] Phosphorescence quenching of the indicator by the ground triplet state of O_2, in principle, can result in the generation of singlet oxygen ($^1O_2$). $^1O_2$ is highly toxic to cells and is widely used in photodynamic therapy (PDT) for cancer treatment. Additionally, photosensitizers such as metal porphyrins, BODIPY and bacteriochlorin derivatives, which are able to react with O_2 to produce $^1O_2$, have been demonstrated to possess therapeutic abilities, some of which have obtained approval for clinical use.[8,9] Thus, it is quite possible to develop a system capable of both hypoxia sensing and PDT treatment. Although such integrative system for diagnosis and therapy is highly desirable in the biomedical field, it is rather challenging owing to the difficulty in combining all the essential features under hypoxia conditions. To date, only a few oxygen sensors based on CPNs have been reported to realize multiple functions for both hypoxia sensing, imaging and treatment.[7] However, these sensors contain polymers that require tedious synthesis procedures and are probably not biodegradable.

Supramolecular polymers are a class of polymers that are assembled *via* low-molecular-weight monomers through reversible non-covalent interactions.[10–13] Previously, we developed ureidopyrimidinone (UPy)-based quadruple hydrogen bonded supramolecular polymer nanoparticles (SPNPs).[14] SPNPs exhibit the same merits of CPNs, such as excellent photostability and good biocompatibility. Moreover, SPNPs possess several unique characteristics. (1) The functionalities of SPNPs are mainly determined by their small monomeric units, and they can be finely tuned through synthetic manipulations.[11a,b] (2) The non-covalent interactions between their small molecular monomers endow the SPNPs potential biodegradability after a reasonable period. (3) SPNPs with a uniform small particle size can be readily dispersed in aqueous solution and can penetrate cells.[14c]

[a] *Key Laboratory of Photochemical Conversion and Optoelectronic Materials, Technical Institute of Physics and Chemistry & University of Chinese Academy of Sciences, Chinese Academy of Sciences, Beijing 100190, China. E-mail: chenyuzhe@mail.ipc.ac.cn, lzwu@mail.ipc.ac.cn*

[b] *Department of Chemistry, University of Miami, Coral Gables, Florida 33146-0431, USA*

† Electronic supplementary information (ESI) available: Synthesis and characterization of compounds, photophysical parameters, energy transfer calculations and other materials. See DOI: 10.1039/c8qm00309b

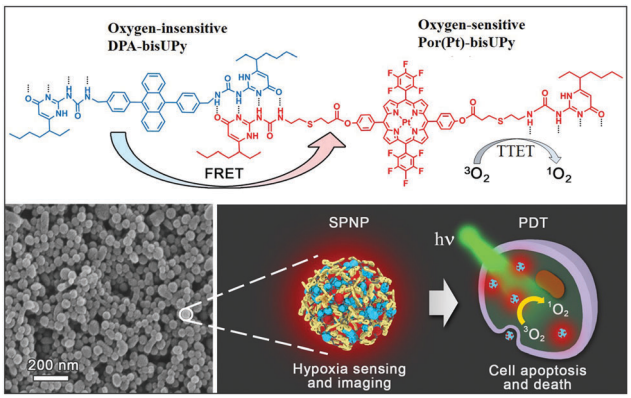

Fig. 1 Chemical structures of Por(Pt)-bisUPy and DPA-bisUPy. SEM image of SPNPs and schematic of the dual-emissive SPNPs for hypoxia sensing, imaging and PDT treatment.

(4) The occurrence of fluorescence resonance energy transfer (FRET) between the appropriate donors and acceptors built into SPNP has been established.[14a,b]

In the present study, we designed a supramolecular polymer nanoparticle (SPNP)-based O_2 nanoprobe for ratiometric hypoxia sensing and cancer therapy. An oxygen-insensitive fluorescence reference moiety bearing bis-ureidopyrimidinone (bis-UPy) acts as the energy donor (D), and an oxygen-sensitive phosphorescence indicator moiety bearing bis-UPy acts as the energy acceptor (A). We assembled these fluorescence and phosphorescence monomeric units into SPNPs through quadruple hydrogen bonding between UPy. The resulting SPNPs can be readily dispersed in aqueous solution and can penetrate cells. Efficient FRET among the D–A pairs in the SPNPs is greatly facilitated, resulting in drastic phosphorescence enhancement. Importantly, the triplet–triplet energy transfer (TTET) from the phosphorescent SPNPs to O_2 enables sensitive ratiometric hypoxia sensing both in aqueous solution and in living cells as well as effective apoptosis of cancer cells by the generated $^1O_2$ (Fig. 1). The results presented demonstrate that SPNPs are excellent luminescent nanoprobes for practical application in determining O_2 concentration in biological systems and effective PDT agents in the treatment of cancer cells.

Results and discussion

Assembly and characterization of SPNPs

The SPNPs we developed for ratiometric O_2 sensing with FRET mediated phosphorescence contain two components: a UPy-containing 9,10-diphenyl anthracene unit (DPA-bisUPy) and a UPy-containing fluorinated phenyl of Pt(II) porphyrin [Por(Pt)-bisUPy]. The former acts as the fluorescence reference dye and energy donor and the latter as a phosphorescence indicator and energy acceptor. Por(Pt)-bisUPy was synthesized in ~60% yield *via* the facile Michael addition of UPy-SH to alkene substituted Pt(II) porphyrin complexes at room temperature. Por(Pt)-bisUPy was characterized thoroughly *via* $^1H/^{13}C$ NMR and HR-MS (see Experimental section and ESI† for details). DPA-bisUPy was synthesized in high yield from 9,10-dibromoanthracene in a few steps. The water-dispersible nanoparticles containing two UPy monomers were prepared following a previously reported method.[14a] The important role of the strong quadruple hydrogen bonding ($K_a = 10^7$ M^{-1} in $CHCl_3$) between UPy in construction of SPNPs has been established.[14a] SPNPs with different molar ratios of Por(Pt)-bisUPy and DPA-bisUPy (1 : 30, 1 : 40, and 1 : 60) were prepared. The morphological studies conducted *via* transmission electron microscopy (TEM) and scanning electron microscopy (SEM) show that stable nanospheres with an average diameter of 70 nm were formed using different molar ratios of DPA-bisUPy and Por(Pt)-bisUPy. The dynamic light scattering measurements (DLS) indicate that the hydrodynamic diameter of the SPNPs is *ca.* 96 nm. The SPNPs stabilized by cationic cetyltrimethyl ammonium bromide (CTAB) surfactant have a zeta potential of +16.1 mV. Furthermore, no significant changes in the size and charge of the nanoparticles with different ratios of DPA-bisUPy and Por(Pt)-bisUPy were observed (Fig. 2a, b and Fig. S1, ESI†).

Photophysical studies of SPNPs

Fig. 2c shows the absorption spectra of the SPNPs composed of Por(Pt)-bisUPy and DPA-bisUPy in aqueous solution. The absorption bands at 350–430 nm are attributed to DPA-bisUPy and the Soret band of the Por(Pt)-bisUPy moiety. The bands at 510 nm and 542 nm are attributed to the Q (1,0) and Q (0,0) bands of the Por(Pt)-bisUPy moiety, respectively. Excitation of the SPNPs at 400 nm resulted in fluorescence at 434 nm from DPA-bisUPy and phosphorescence at 660 nm from Por(Pt)-bisUPy. Owing to the substantial overlap between the absorption bands

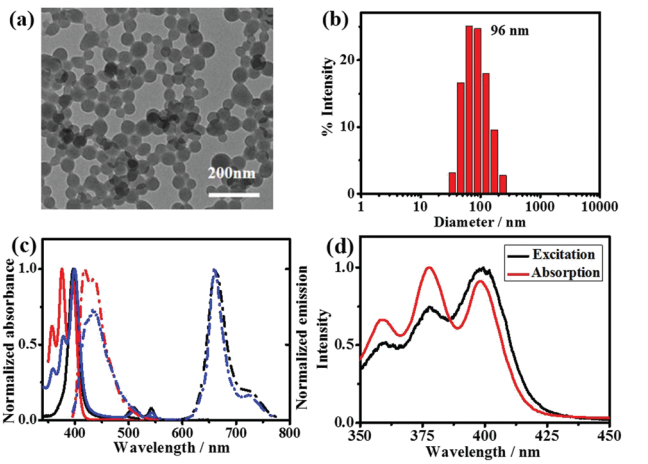

Fig. 2 TEM image (a) and DLS analysis (b) of SPNPs with a molar ratio of 40 : 1 DPA-bisUPy and Por(Pt)-bisUPy. (c) Normalized absorption and emission spectra of monomers DPA-bisUPy ($c = 1.6 \times 10^{-5}$ M) and Por(Pt)-bisUPy ($c = 3.0 \times 10^{-6}$ M) in chloroform and SPNPs (D/A = 40/1) in aqueous solution ($c = 1.7 \times 10^{-6}$ M). Black line: absorption of Por(Pt)-bisUPy, red line: absorption of DPA-bisUPy, blue line: absorption of SPNPs, black dotted line: phosphorescence of Por(Pt)-bisUPy (λ_{ex} = 400 nm), red dotted line: fluorescence of DPA-bisUPy (λ_{ex} = 375 nm) and blue dotted line: emission of SPNPs (λ_{ex} = 375 nm). (d) Normalized excitation spectrum of SPNPs-dispersed aqueous solution ([D]/[A] = 60 : 1) and normalized absorption spectrum of DPA-bisUPy in $CHCl_3$.

of Por(Pt)-bisUPy (375–430 nm) and the emission bands of DPA-bisUPy (400–550 nm) as well as the short D–A distance resulting from the hydrogen bonding interactions in SPNPs, the FRET process from DPA-bisUPy to Por(Pt)-bisUPy was confirmed by recording the emission spectra of SPNPs with different ratios of donor and acceptor while maintaining the same absorption intensity at 375 nm (Fig. S2a, ESI†). As shown in Fig. S2b (ESI†), upon selective excitation at 375 nm, an increase in the A/D molar ratio from 1/60 to 1/30 lowered the fluorescence intensity at 434 nm, but enhanced the phosphorescence intensity at 660 nm. The excitation spectrum of the SPNPs at 660 nm matches the absorption spectrum of DPA-bisUPy, indicating that the emission was contributed mainly by DPA-bisUPy (Fig. 2d). The energy-transfer efficiency (Φ_{ET}) of the three SPNPs was 96.8%, 94.4% and 89.3%, respectively. The Förster radius (r_0) was estimated to be 3.4 nm for the D–A pair (see ESI† for details). The phosphorescence quantum yield of the Por(Pt)-bisUPy monomer in chloroform is 0.4%, which was enhanced by more than 14-times to 5.7% in an aqueous solution of the SPNPs (D/A = 40 : 1) due to the light harvesting effect from the FRET process.[15] The photophysical properties of the monomers and SPNPs were studied and listed in the ESI† in Table S1. The phosphorescence lifetime of the SPNPs-dispersed aqueous solution was found to be 70.3 μs at 660 nm under nitrogen atmosphere, which is a significant enhancement from that of the platinum(II)porphyrin moiety in chloroform (τ = 36.4 μs) and conjugated polymers (34.7 μs).[7a] This might be attributed to the suppression of the aggregation and free motion of Por(Pt)-bisUPy by the rigid supramolecular backbone. Higher phosphorescence quantum yield and longer phosphorescence lifetime are beneficial for sensitive O_2 detection and efficient $^1O_2$ production.

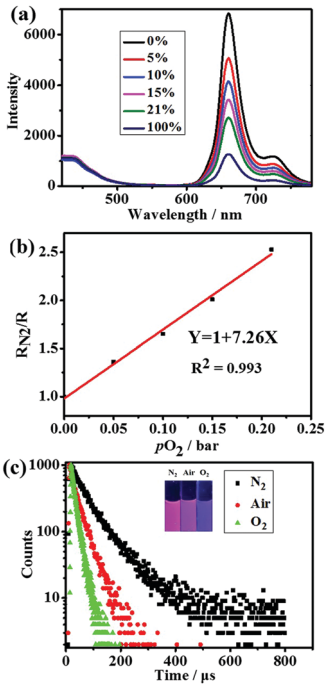

Fig. 3 (a) Ratiometric emission responses of the aqueous solution of SPNPs (D/A = 40 : 1) under different oxygen partial pressures (0%, 5%, 10%, 15%, 21%, and 100% bar) (λ_{ex} = 400 nm). (b) Stern–Volmer plot of R_{N_2}/R *vs.* different O_2 partial pressures. (c) Luminescence decays at 660 nm of the SPNPs in water under oxygen, air and nitrogen atmospheres (λ_{ex} = 400 nm). The concentration of the SPNPs expressed by DPA-bisUPy is 2.7 × 10^{-5} M. Inset: Emission colors of the SPNPs-dispersed aqueous solution with different gas atmospheres under a 365 nm UV lamp.

Hypoxia sensing and imaging

The luminescence spectra of SPNPs in water under different O_2 partial pressures are presented in Fig. 3a. The D to A ratio of 40 : 1 in SPNPs exhibited appropriate fluorescence to phosphorescence signal ratios. The fluorescence at 434 nm associated with the DPA-bisUPy moiety was almost unchanged, while the phosphorescence at 660 nm from the Por(Pt)-bisUPy moiety decreased markedly with an increase in partial pressure of O_2. As a result, the ratio of phosphorescence to fluorescence intensity in the SPNPs is dependent on the O_2 concentration. The red phosphorescence at 660 nm became dominant under 0% O_2 atmosphere in the presence of efficient FRET from the singlet excited state of DPA-bisUPy to the Por(Pt)-bisUPy moieties. Upon increasing the O_2 partial pressure, the emission colors of the aqueous solution changed from pink to purple, which can be visualized under a 365 nm UV lamp by the naked eyes (inset of Fig. 3c). The ratiometric O_2 sensing was analyzed quantitatively according to the Stern–Volmer equation based on the data shown in Fig. 3b.

$$\frac{R_0}{R} = 1 + K_{S-V}PO_2 \quad (1)$$

where R and R_0 are the ratios of the emission intensities of phosphorescence at 660 nm and fluorescence at 434 nm in the presence and absence of O_2, respectively, PO_2 is the O_2 partial pressure, and K_{S-V} represents the Stern–Volmer constant of the plot involving R_0/R and PO_2. As shown in Fig. 3b, there is a linear relationship between R_0/R and PO_2, from which K_{S-V} was estimated to be 7.26 bar^{-1}. The O_2 partial pressure in aqueous solution was determined using this K_{S-V} value. The high sensitivity of the SPNPs could be expressed as the Q factor from the total response to O_2, which was measured to be 82.6% (see ESI† for details). The phosphorescence quenching by O_2 is rapid and reversible by N_2 bubbling, revealing the reusability of the system. The phosphorescence quenching process by collision with O_2 was further confirmed by measuring the phosphorescence lifetimes at 660 nm, which were 15.7 μs, 32.3 μs and 70.3 μs for the SPNPs-dispersed aqueous solutions under O_2, air and N_2 atmosphere, respectively (Fig. 3c).

Imaging of intracellular O_2 levels by SPNPs in HeLa cells was investigated *via* confocal laser scanning microscopy (CLSM). HeLa cells were cultured with the SPNPs, and then incubated under 1% and 21% O_2 atmosphere at 37 °C. Upon excitation at 405 nm, the signals for fluorescence (430–470 nm, I_{blue}) and phosphorescence (660–740 nm, I_{red}) were collected in two separate channels. The outstanding ratiometric intracellular O_2 detection properties of the SPNPs are evident from the changes in the I_{blue}/I_{red} ratio values in HeLa cells cultured under 21% and 1% oxygen atmosphere (Fig. 4).

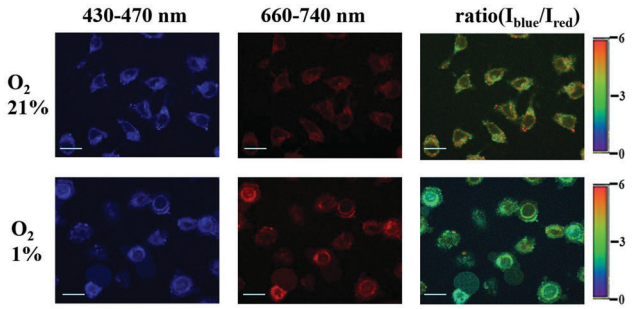

Fig. 4 Ratiometric confocal luminescence images of HeLa cells cultured with SPNPs (1.8×10^{-6} M in water) under 1% and 21% O_2 partial pressure. The ratio between the emission intensities at 430–470 nm to that at 660–740 nm (I_{blue}/I_{red}) was set as the detection signal (λ_{ex} = 405 nm), scale bar: 20 μm.

Photoinduced cytotoxicity by the PDT process

Next, the electron spin resonance spectra (ESR) were recorded to verify the generation of $^1O_2$. For this purpose, $^1O_2$ was trapped with the well-known scavenger 2,2,6,6-tetramethylpiperidine (TEMP).[16] As shown in Fig. 5a, upon irradiation of a mixture of TEMP and SPNPs-dispersed aqueous solution for 5 min, ESR signals of the $^1O_2$ adduct was detected. The quantum yield of $^1O_2$ generation was measured *via* chemical trapping with 1,3-diphenylbenzofuran (DPBF)[17] and Rose Bengal (RB) as the standard photosensitizer (Φ_{RB} = 0.80 in MeOH) under 532 nm laser irradiation.[18] As illustrated in Fig. 5b and Fig. S3 (ESI†), the absorption due to the DPBF solution at a wavelength of 418 nm decreased linearly over 60 s of irradiation. This suggests that $^1O_2$ was generated efficiently upon direct excitation of the Q band of the Por(Pt)-bisUPy moiety in the SPNPs. The $^1O_2$ quantum yield was calculated to be 0.70 (Fig. 5c).

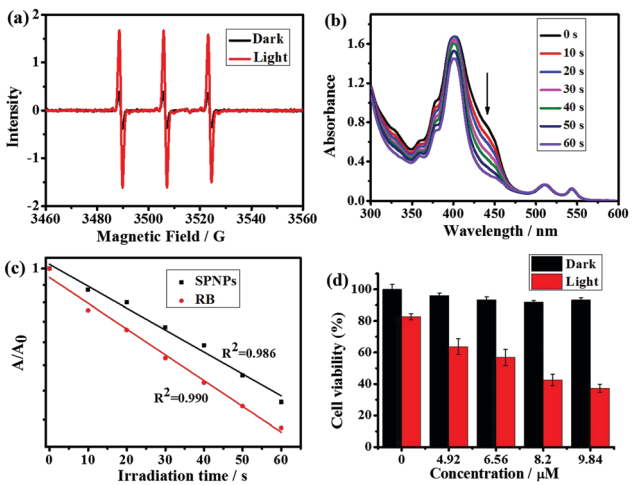

Fig. 5 (a) ESR spectra of an aqueous solution of SPNPs (4.1×10^{-4} M) and TEMP (3 μL) upon photoirradiation by an Xe lamp at >400 nm for 0 min and 5 min under air. (b) UV-vis absorption spectra of SPNPs (1.4×10^{-4} M) and DPBF (40 μL) upon irradiation by a 532 nm laser. (c) Plots of the optical density changes of DPBF at 418 nm in the presence of SPNPs and RB *versus* irradiation time. (d) CCK-8 cell viabilities of HeLa cells incubated with SPNPs at various concentrations and then irradiated with an Xe lamp (>400 nm, 30 mW) for 30 min. The concentrations of the SPNPs are expressed using DPA-bisUPy, in which [D]/[A] = 40 : 1.

To evaluate the PDT performance of the SPNPs quantitatively, the photoinduced cytotoxicity of the SPNPs in HeLa cells was measured using the standard Cell Counting Kit-8 assay (CCK-8) at various concentrations (0–9.84 μM). As shown in Fig. 5d, under the PDT process, prominent cytotoxicity was revealed. Upon increasing the sample concentration to 9.84 μM, the viability of the cells decreased to 37%. However, the SPNPs had a negligible effect on the viability of the cells in the dark, confirming the need for light in the process. The PDT effects of the SPNPs against cancer cells were further studied by monitoring the morphological variations in the HeLa cells with SPNPs under 514 nm laser irradiation using CLSM. As illustrated in Fig. S4 (ESI†), the morphology of the cells changed significantly upon laser irradiation, with the formation of numerous blebs and shrinkage of the HeLa cells, indicating apoptosis and death of the tumour cells, respectively. In sharp contrast, no significant morphological changes in the cancer cells were observed without SPNPs under the same conditions, suggesting that the SPNPs efficiently generated $^1O_2$ upon laser irradiation. Furthermore, the SPNPs exhibited superior storage stability and photostability, which are critical in biomedical applications (Fig. S5 and see ESI† for details).

Conclusions

In summary, we presented our design of a multifunctional SPNPs-based O_2 nanoprobe for ratiometric hypoxia sensing, imaging and therapy. The nanoprobe was assembled by a phosphorescent Pt(II) porphyrin unit and fluorescent 9,10-diphenylanthracene moiety through quadruple hydrogen bonding. Bright phosphorescence with long lifetime was facilitated by the efficient energy transfer in the nanoprobe, resulting in sensitive ratiometric hypoxia sensing both in solution and in living cells. More importantly, the singlet oxygen generated during the quenching process also causes damage to cancer cells. The SPNPs possess the advantages of easy preparation and structural modulation, good water-dispersibility, excellent stability, and low dark cytotoxicity toward living cells. The preliminary experiments demonstrate the great potential of SPNP-based integrated systems for diagnosis therapy in the biomedical field. The investigation of SPNPs in PDT for near-infrared multi-photon excitation is currently underway.

Experimental section

Synthesis

DPA-bisUPy was prepared in high yield according to the reported procedure.[14a] Por(Pt)-bisUPy was synthesized following the steps outlined in Scheme S1 (ESI†).

Synthesis of Por(Pt)-bisUPy: a mixture of P4 (100 mg, 0.089 mmol), UPy-SH (75 mg, 0.235 mmol) and triethylamine (0.1 mL) in CH_2Cl_2 (50 mL) was stirred under N_2 at room temperature for 24 h. After evaporation of the solvent, the

product was purified *via* gel chromatography using CH_2Cl_2/CH_3OH (100 : 1, v/v) as the eluent to afford 0.06 g of the product. Yield: 60%. ^{1}H NMR (400 MHz, $CDCl_3$): δ (ppm) = 0.87–0.91(m, 12H), 1.27(s, 8H), 1.58–1.67(m, 8H), 2.34(s, 2H), 2.94–3.10(m, 12H), 3.60–3.61(m, 4H), 5.90(s, 2H), 7.50–7.52(d, 4 H, J = 6.8 Hz), 8.15–8.17(d, 4H, J = 7.2 Hz), 8.72–8.73(d, 4H, J = 3.6 Hz), 8.88–8.90(d, 4H, J = 4.0 Hz), 10.60(s, 2H), 12.09(s, 2H), 13.21(s, 2H). ^{13}C NMR (100 MHz, $CDCl_3$): δ 11.76, 13.91, 14.16, 22.57, 22.77, 25.66, 26.75, 27.24, 27.34, 29.43, 29.71, 29.80, 29.89, 31.66, 32.02, 32.99, 35.41, 40.07, 45.51, 106.45, 120.31, 122.55, 129.43, 132.62, 134.80, 138.23, 140.59, 141.60, 151.10, 154.99, 155.82, 157.07, 170.56, 173.29. HR-ESI-MS: m/z calculated for $[M + H]^+$ $C_{78}H_{71}F_{10}N_{12}O_8PtS_2$: 1752.4424, found 1752.4442.

Preparation of SPNPs

SPNPs with different molar ratios of Por(Pt)-bisUPy and DPA-bisUPy (1 : 30, 1 : 40, 1 : 60) were prepared by following the general method outlined below for a solution of 1 : 40 molar ratio of Por(Pt)-bisUPy and DPA-bisUPy: a mixture of Por(Pt)-bisUPy (0.24 mg, 0.14 mmol) and DPA-bisUPy (4.76 mg, 5.54 mmol) in 200 μL of $CHCl_3$ was quickly injected into 10 mL of CTAB aqueous solution (1.0×10^{-3} M), sonicated for 25 min, centrifuged and washed with water three times to afford uniform nanoparticles.

The concentration of the SPNPs in aqueous solution is expressed by the DPA-bisUPy concentration. Different concentrations of SPNPs in water were prepared by diluting the concentrated stock aqueous solution of SPNPs. Lifetime and quantum yield measurements were performed by carefully degassing all solutions.

Phosphorescence quantum yield measurements

The phosphorescence quantum yield was measured using $[Ru(bpy)_3]Cl_2$ (Φ = 0.094 in deoxygenated acetonitrile) as the standard according to the literature procedure.[19,20]

$$\Phi = \Phi_s \times \left(\frac{F}{F_s}\right) \times \left(\frac{A_S}{A}\right) \times \left(\frac{n^2}{n_s^2}\right) \quad (2)$$

In eqn (2), Φ represents the quantum yield, F denotes the integrated phosphorescence intensity, n represents the refractive index, and A is the optical density. The subscript S stands for the standard.

Measurement of quantum yield for $^1O_2$ generation

RB and DPBF were used as the singlet oxygen photosensitizer and $^1O_2$-trapping agent, respectively. In the experiments, 40 μL DPBF solution (0.75 mg mL^{-1} in MeOH) was added to 2 mL SPNP-dispersed aqueous solution (1.4×10^{-4} M) and photoirradiated under a 532 nm laser at a power of 40 mW. The reaction decay rate was obtained by recording the absorption of DPBF at 418 nm at different irradiation times. The $^1O_2$ quantum yield was calculated using eqn (3):

$$\Phi_{\Delta(x)} = \Phi_{\Delta(RB)} \frac{S_x}{S_{RB}} \frac{F_{RB}}{F_x} \quad (3)$$

where subscripts x and RB denote the nanoprobe and RB, respectively, and S represents the linear slope of the plot of DPBF absorbance at 418 nm *versus* irradiation time. F, which is given by $F = 1–10^{-OD}$, represents the absorption correction factor (OD stands for the optical density of the SPNPs and RB at 532 nm). $\Phi_{\Delta(RB)}$ is the singlet oxygen quantum yield of RB, and $\Phi_{\Delta(RB)}$ = 0.80 in MeOH. Photoirradiation of the solutions under identical conditions but in the absence of either photosensitizer or light induced negligible absorption changes.

Cytotoxicity of SPNPs

The dark cytotoxicity and photocytoxicity of the SPNPs on HeLa cells were evaluated using the standard CCK-8 assay. The SPNPs-dispersed aqueous solution was diluted to various concentrations (0, 4.92, 6.56, 8.20 and 9.84 μM) with DMEM medium containing 5% FBS. The HeLa cells were then incubated with the above solutions under 5% CO_2 at 37 °C for 4 h. After removing the medium, the HeLa cells were washed with fresh medium twice to remove free SPNPs, and irradiated by a Xe lamp at an intensity of 30 mW for 0 or 30 min. Following this, fresh growth medium (100 μL) containing CCK-8 (10 μL) was added to each well. Upon 20 h incubation, the absorbance intensity at 450 nm was recorded using a microplate reader. The control wells did not include SPNPs. The reference point of 100% cell viability was established by the absorbance of an untreated cell population under identical experimental conditions. The ratio between the average absorption intensities of the sample wells and control wells, $[A]_{sample}/[A]_{control}$, was calculated to obtain the cell viability relative to the control.

Conflicts of interest

There are no conflicts to declare.

Acknowledgements

Financial support from the Ministry of Science and Technology of China (2014CB239402 and 2017YFA0206903), the National Natural Science Foundation of China (21474124, 21390404 and 91427303), the Strategic Priority Research Program of the Chinese Academy of Sciences (XDB17000000), the Key Research Program of Frontier Sciences of the Chinese Academy of Sciences (QYZDY-SSW-JSC029) are gratefully acknowledged. V. Ramamurthy acknowledges K. C. Wong Education Foundation for the research support.

Notes and references

1 (*a*) G. L. Semenza, Life with Oxygen, *Science*, 2007, **318**, 62–64; (*b*) J. Aragones, P. Fraisl, M. Baes and P. Carmeliet, Oxygen Sensors at the Crossroad of Metabolism, *Cell Metab.*, 2009, **9**, 11–22.

2 (*a*) P. Carmeliet, Y. Dor, J. M. Herbert, D. Fukumura, K. Brusselmans, M. Dewerchin, M. Neeman, F. Bono, R. Abramovitch, P. Maxwell, C. J. Koch, P. Ratcliffe, L. Moons, R. K. Jain, D. Collen and E. Keshet, Role of HIF-1α in Hypoxia-Mediated Apoptosis, Cell Proliferation and Tumour Angiogenesis, *Nature*, 1998, **394**, 485–490; (*b*) A. H. V. Schapira,

Lancet, 2012, **379**, 1825–1834; (*c*) J. E. Selfridge, L. E. J. H. Lu and R. H. Swerdlow, Role of Mitochondrial Homeostasis and Dynamics in Alzheimer's Disease, *Neurobiol. Dis.*, 2013, **51**, 3–12.

3 (*a*) X.-D. Wang and O. S. Wolfbeis, Optical Methods for Sensing and Imaging Oxygen: Materials, Spectroscopies and Applications, *Chem. Soc. Rev.*, 2014, **43**, 3666–3761; (*b*) D. B. Papkovsky and R. I. Dmitriev, Biological Detection by Optical Oxygen Sensing, *Chem. Soc. Rev.*, 2013, **42**, 8700–8732; (*c*) Y. Feng, J. Cheng, L. Zhou, X. Zhou and H. Xiang, Ratiometric Optical Oxygen Sensing: a Review in Respect of Material Design, *Analyst*, 2012, **137**, 4885–4901.

4 (*a*) Y.-E. L. Koo, Y. Cao, R. Kopelman, S. M. Koo, M. Brasuel and M. A. Philbert, Real-Time Measurements of Dissolved Oxygen Inside Live Cells by Organically Modified Silicate Fluorescent Nanosensors, *Anal. Chem.*, 2004, **76**, 2498–2505; (*b*) X.-d. Wang, J. A. Stolwijk, T. Lang, M. Sperber, J. Wegener and O. S. Wolfbeis, Ultra-Small, Highly Stable, and Sensitive Dual Nanosensors for Imaging Intracellular Oxygen and pH in Cytosol, *J. Am. Chem. Soc.*, 2012, **134**, 17011–17014; (*c*) J. N. Liu, Y. Liu, W. B. Bu, J. W. Bu, Y. Sun, J. L. Du and J. L. Shi, Ultrasensitive Nanosensors based on Upconversion Nanoparticles for Selective Hypoxia Imaging in Vivo upon Near-Infrared Excitation, *J. Am. Chem. Soc.*, 2014, **136**, 9701–9709.

5 C. M. Lemon, P. N. Curtin, R. C. Somers, A. B. Greytak, R. M. Lanning, R. K. Jain, M. G. Bawendi and D. G. Nocera, Metabolic Tumor Profiling with pH, Oxygen, and Glucose Chemosensors on a Quantum Dot Scaffold, *Inorg. Chem.*, 2014, **53**, 1900–1915.

6 (*a*) R. Xu, Y. Wang, X. Duan, K. Lu, D. Micheroni, A. Hu and W. Lin, Nanoscale Metal-Organic Frameworks for Ratiometric Oxygen Sensing in Live Cells, *J. Am. Chem. Soc.*, 2016, **138**, 2158–2161; (*b*) C. F. Wu, B. Bull, K. Christensen and J. McNeill, Ratiometric Single-Nanoparticle Oxygen Sensors for Biological Imaging, *Angew. Chem., Int. Ed.*, 2009, **48**, 2741–2745.

7 (*a*) X. B. Zhou, H. Liang, P. F. Jiang, K. Y. Zhang, S. J. Liu, T. S. Yang, Q. Zhao, L. J. Yang, W. Lv, Q. Yu and W. Huang, Multifunctional Phosphorescent Conjugated Polymer Dots for Hypoxia Imaging and Photodynamic Therapy of Cancer Cells, *Adv. Sci.*, 2016, **3**, 1500155; (*b*) H. Shi, X. Ma, Q. Zhao, B. Liu, Q. Qu, Z. An, Y. Zhao and W. Huang, Ultrasmall Phosphorescent Polymer Dots for Ratiometric Oxygen Sensing and Photodynamic Cancer Therapy, *Adv. Funct. Mater.*, 2014, **24**, 4823–4830; (*c*) Z. Lv, L. Zou, H. Wei, S. Liu, W. Huang and Q. Zhao, Phosphorescent Starburst Pt(ii) Porphyrins as Bifunctional Therapeutic Agents for Tumor Hypoxia Imaging and Photodynamic Therapy, *ACS Appl. Mater. Interfaces*, 2018, **10**, 19523–19533; (*d*) Z. Feng, P. Tao, L. Zou, P. Gao, Y. Liu, X. Liu, H. Wang, S. Liu, Q. Dong, J. Li, B. Xu, W. Huang, W.-Y. Wong and Q. Zhao, Hyperbranched Phosphorescent Conjugated Polymer Dots with Iridium(III) Complex as the Core for Hypoxia Imaging and Photodynamic Therapy, *ACS Appl. Mater. Interfaces*, 2017, **9**, 28319–28330.

8 (*a*) S. S. Lucky, K. C. Soo and Y. Zhang, Nanoparticles in Photodynamic Therapy, *Chem. Rev.*, 2015, **115**, 1990–2042; (*b*) Y. Shen, A. J. Shuhendler, D. Ye, J.-J. Xu and H.-Y. Chen, Two-Photon Excitation Nanoparticles for Photodynamic Therapy, *Chem. Soc. Rev.*, 2016, **45**, 6725–6741; (*c*) C. Zhu, L. Liu, Q. Yang, F. Lv and S. Wang, Water-Soluble Conjugated Polymers for Imaging, Diagnosis, and Therapy, *Chem. Rev.*, 2012, **112**, 4687–4735; (*d*) L. Chen, H. Bai, Q. Song, J.-F. Xu, S. Wang and X. Zhang, Supramolecular Porphyrin Photosensitizers: Controllable Disguise and Photo-induced Activation of Antibacterial Behavior, *ACS Appl. Mater. Interfaces*, 2017, **9**, 13950–13957.

9 (*a*) M. Ethirajan, Y. Chen, P. Joshi and R. K. Pandey, The Role of Porphyrin Chemistry in Tumor Imaging and Photodynamic Therapy, *Chem. Soc. Rev.*, 2011, **40**, 340–362; (*b*) S. Singh, A. Aggarwal, N. V. S. D. K. Bhupathiraju, G. Arianna, K. Tiwari and C. M. Drain, Glycosylated Porphyrins, Phthalocyanines, and Other Porphyrinoids for Diagnostics and Therapeutics, *Chem. Rev.*, 2015, **115**, 10261–10306; (*c*) J. P. Celli, B. Q. Spring, I. Rizvi, C. L. Evans, K. S. Samkoe, S. Verma, B. W. Pogue and T. Hasan, Imaging and Photodynamic Therapy: Mechanisms, Monitoring, and Optimization, *Chem. Rev.*, 2010, **110**, 2795–2838; (*d*) J. Zhao, K. Xu, W. Yang, Z. Wang and F. Zhong, The Triplet Excited State of Bodipy: Formation, Modulation and Application, *Chem. Soc. Rev.*, 2015, **44**, 8904–8939; (*e*) A. Kamkaew, S. H. Lim, H. B. Lee, L. V. Kiew, L. Y. Chung and K. Burgess, BODIPY Dyes in Photodynamic Therapy, *Chem. Soc. Rev.*, 2013, **42**, 77–88.

10 (*a*) R. P. Sijbesma, F. H. Beijer, L. Brunsveld, B. J. B. Folmer, J. H. K. Ky Hirschberg, R. F. M. Lange, J. K. L. Lowe and E. W. Meijer, Reversible Polymers Formed from Self-Complementary Monomers Using Quadruple Hydrogen Bonding, *Science*, 1997, **278**, 1601–1604; (*b*) S.-G. Chen, Y. Yu, X. Zhao, Y. Ma, X.-K. Jiang and Z.-T. Li, Highly Stable Chiral $(A)_6$–B Supramolecular Copolymers: A Multivalency-Based Self-Assembly Process, *J. Am. Chem. Soc.*, 2011, **133**, 11124–11127.

11 (*a*) L. Yang, X. Tan, Z. Wang and X. Zhang, Supramolecular Polymers: Historical Development, Preparation, Characterization, and Functions, *Chem. Rev.*, 2015, **115**, 7196–7239; (*b*) T. Aida, E. W. Meijer and S. I. Stupp, Functional Supramolecular Polymers, *Science*, 2012, **335**, 813–817; (*c*) C. Fouquey, J. M. Lehn and A. M. Levelut, Molecular Recognition Directed Self-assembly of Supramolecular Liquid Crystalline Polymers from Complementary Chiral Components, *Adv. Mater.*, 1990, **2**, 254–257.

12 (*a*) J. D. Barrio, P. N. Horton, D. Lairez, G. O. Lloyd, C. Toprakcioglu and O. A. Scherman, Photocontrol over Cucurbit [8] uril Complexes: Stoichiometry and Supramolecular Polymers, *J. Am. Chem. Soc.*, 2013, **135**, 11760–11763; (*b*) Y. Wang, C.-L. Sun, L.-Y. Niu, L.-Z. Wu, C.-H. Tung, Y.-Z. Chen and Q.-Z. Yang, Photoresponsive AA/BB Supramolecular polymers Comprising Stiff-stilbene Based Guests and Bispillar [5] arenes, *Polym. Chem.*, 2017, **8**, 3596–3602.

13 (*a*) G. Yu, X. Zhao, J. Zhou, Z. Mao, X. Huang, Z. Wang, B. Hua, Y. Liu, F. Zhang, Z. He, O. Jacobson, C. Gao, W. Wang, C. Yu, X. Zhu, F. Huang and X. Chen, Supramolecular Polymer-Based Nanomedicine: High Therapeutic Performance and Negligible Long-Term Immunotoxicity,

J. Am. Chem. Soc., 2018, **140**, 8005–8019; (*b*) M. Ni, N. Zhang, W. Xia, X. Wu, C. Yao, X. Liu, X.-Y. Hu, C. Lin and L. Wang, Dramatically Promoted Swelling of a Hydrogel by Pillar[6]arene–Ferrocene Complexation with Multistimuli Responsiveness, *J. Am. Chem. Soc.*, 2016, **138**, 6643–6649.

14 (*a*) H.-Q. Peng, J.-F. Xu, Y.-Z. Chen, L.-Z. Wu, C.-H. Tung and Q.-Z. Yang, Water-Dispersible Nanospheres of Hydrogen-Bonded Supramolecular Polymers and their application for mimicking light-harvesting systems, *Chem. Commun.*, 2014, **50**, 1334–1337; (*b*) H.-Q. Peng, C.-L. Sun, L.-Y. Niu, Y.-Z. Chen, L.-Z. Wu, C.-H. Tung and Q.-Z. Yang, Supramolecular Polymeric Fluorescent Nanoparticles based on Quadruple Hydrogen Bonds, *Adv. Funct. Mater.*, 2016, **26**, 5483–5489; (*c*) R.-F. Wang, H.-Q. Peng, P.-Z. Chen, L.-Y. Niu, J.-F. Gao, L.-Z. Wu, C.-H. Tung, Y.-Z. Chen and Q.-Z. Yang, A Hydrogen-Bonded-Supramolecular-Polymer-Based Nanoprobe for Ratiometric Oxygen Sensing in Living Cells, *Adv. Funct. Mater.*, 2016, **26**, 5419–5425; (*d*) F.-W. Liu, L.-Y. Niu, Y. Chen, V. Ramamurthy, L.-Z. Wu, C.-H. Tung, Y.-Z. Chen and Q.-Z. Yang, A Phosphorescent Platinum(II) Bipyridyl Supramolecular Polymer Based on Quadruple Hydrogen Bonds, *Chem. – Eur. J.*, 2016, **22**, 18132–18139.

15 H.-Q. Peng, Y.-Z. Chen, Y. Zhao, Q.-Z. Yang, L.-Z. Wu, C.-H. Tung, L.-P. Zhang and Q.-X. Tong, Artificial Light-Harvesting System Based on Multifunctional Surface-Cross-Linked Micelles, *Angew. Chem., Int. Ed.*, 2012, **51**, 2088–2092.

16 J. Ge, M. Lan, B. Zhou, W. Liu, L. Guo, H. Wang, Q. Jia, G. Niu, X. Huang, H. Zhou, X. Meng, P. Wang, C.-S. Lee, W. Zhang, X. Han and A. Graphene, Quantum Dot Photodynamic Therapy Agent with High Singlet Oxygen Generation, *Nat. Commun.*, 2014, **5**, 4596.

17 N. Adarsh, R. R. Avirah and D. Ramaiah, Tuning Photosensitized Singlet Oxygen Generation Efficiency of Novel Aza-BODIPY Dyes, *Org. Lett.*, 2010, **12**, 5720–5723.

18 L. Xiao, L. Gu, S. B. Howell and M. J. Sailor, Porous Silicon Nanoparticle Photosensitizers for Singlet Oxygen and Their Phototoxicity against Cancer Cells, *ACS Nano*, 2011, **5**, 3651–3659.

19 A. M. Brouwer, Standards for Photoluminescence Quantum Yield Measurements in Solution (IUPAC Technical Report), *Pure Appl. Chem.*, 2011, **83**, 2213–2228.

20 K. Suzuki, A. Kobayashi, S. Kaneko, K. Takehira, T. Yoshihara, H. Ishida, Y. Shiina, S. Oishic and S. Tobita, Reevaluation of Absolute Luminescence Quantum Yields of Standard Solutions Using a Spectrometer with an Integrating Sphere and a Back-Thinned CCD Detector, *Phys. Chem. Chem. Phys.*, 2009, **11**, 9850–9860.